Locked octahedral tilting in orthorhombic perovskites. At the boundary of the general rule predicting phase transitions

M. Ardit[1,*], M. Dondi[2], and G. Cruciani[1]
[1]Department of Physics and Earth Sciences, University of Ferrara, I-44122 Ferrara, Italy
[2]Institute of Science and Technology for Ceramics, CNR-ISTEC, I-48018 Faenza, Italy
[*]To whom correspondence should be addressed. Email address: rdtmtt@unife.it

Mainly ruled by oxygen octahedral rotations, perovskite oxides can exhibit zone boundary transitions (ZBTs) either with $dT_c/dP > 0$ and $dT_c/dP < 0$. Synchrotron structural investigations at high pressure conditions place $YAl_{0.25}Cr_{0.75}O_3$ orthorhombic perovskite at the boundary of ZBTs. The absence of changes in the octahedral tilting and a volume reduction with pressure exclusively controlled by an isotropic polyhedral compression set $YAl_{0.25}Cr_{0.75}O_3$ as the first finding of a possible asymptote at the Clapeyron relation for predicting ZBTs in perovskites. Furthermore, the discovery of a "*locked-tilt perovskite*" can pave the way to a new class of functional materials.

I. INTRODUCTION

The interest in $GdFeO_3$-type perovskite minerals and synthetic analogues evenly spans Geophysics and Materials Science. In fact, at the conditions of the upper/lower mantle interface, olivine, pyroxene, and garnet minerals undergo a series of phase transitions to the denser $(Mg,Fe)SiO_3$ orthorhombic perovskite. Furthermore, at core/mantle boundary conditions, $(Mg,Fe)SiO_3$ perovskite transforms to a more compact layered atomic arrangement known as post-perovskite (s.g. *Cmcm*) [1]. At the same time, the excess physical properties, consequence of structural phase transitions that distort the ideal aristotype structure, promote perovskites to reference compounds in technological applications.

Perovskite oxides, with general stoichiometry ABO_3, are relatively simple crystal structures. The aristotype form is a cubic structure (s.g. *Pm*-3*m*) with *A* cations located at the centre of dodecahedral sites defined by a three-dimensional framework of corner-sharing BO_6 octahedra. Whether orthorhombic (s.g. *Pbnm*), perovskites belong to the so called $GdFeO_3$-type series and derive from the aristotype structure through a combination of two octahedral tilts (i.e. along [110] and [001] directions, respectively) and distortion of the BO_6 octahedra.

Most of the countless physical properties (such as magnetic, electronic, electric, and orbital properties) which characterize the orthorhombic perovskites derive from their chemistry and from the degree of the octahedral tilts [2].

Beyond that, the change in octahedral tilting is the basis for interpreting the variation of the perovskites state with temperature and pressure, and to describe the thermodynamic processes associated with displacive phase transitions (or also called zone boundary transitions, ZBTs) in these compounds [3]. In ZBTs, the atomic displacement associated with the transition of the aristotype cubic phase can be simply described as a change in the tilt system [4]. Angel et al. [3] demonstrated that both the evolution of perovskite compounds with pressure, and the "*general rule*" for predicting the variation in transition temperatures of tilt transitions in perovskites [5], can be interpreted as the combination of the relative compressibility of constituent AO_{12} and BO_6 polyhedra with the octahedral tilts. Depending on the formal charge of the *A* and *B* cations, two possible scenarios can take shape. When *A* has a lower formal charge than *B* (i.e. 2+:4+), the AO_{12} site is more compressible than the BO_6 octahedron, and the volume reduction is associated to an increase of the octahedral tilting. Conversely, when *A* and *B* have the same formal charge (i.e.

3+:3+), the AO_{12} site is stiffer than the BO_6 octahedron, then the volume reduction is partially compensated by a decrease of the octahedral tilting. The thermodynamic counterpart is that, for perovskites 2:4, the Clapeyron equation is satisfied for $dT_c/dP = \Delta S/\Delta V > 0$ (with T_c as the phase transition temperature), meaning that both entropy and volume increase; whereas for perovskites 3:3, the Clapeyron equation is satisfied for $dT_c/dP = \Delta S/\Delta V < 0$, i.e. by an increase in entropy but a decrease in volume [3].

On the other hand, as reported by Guennou et al. [6], the evidence that the octahedral tilting can either increase or decrease with increasing pressure, is a challenge to the search for a perovskite in which the tilt angles do not change with pressure, but where the compression is largely dominated by bond compression.

The analysis of a series of $YM^{3+}O_3$ isotype perovskites paved the way to a possible perovskite whose lattice distortion will neither increase nor decrease under compression [7]. In particular, it was suggested that this $GdFeO_3$-type perovskite should possess a mean octahedral bond angle $\langle B\square O\square B\rangle$ of about 147° and, in the case of a $YM^{3+}O_3$ isotype, a ionic radius of the M^{3+} ion at the B site of about 0.59 Å [7]. Later on, it was pointed out that a compound with such features could be a perovskite with composition $YAl_{0.25}Cr_{0.75}O_3$ [8].

Besides to be situated at the boundary of the "*general rule*" as modified by Angel and coauthors [3], and hence open another possible thermodynamic scenario, a compound that retains its degree of octahedral tilting unchanged regardless of changes of intensive variables could be extremely promising in several technological applications [9, 10].

In this contribution, the structural modifications of $YAl_{0.25}Cr_{0.75}O_3$ orthorhombic perovskite, obtained through a sol-gel combustion process, have been investigated at high-pressure conditions by means of synchrotron X-ray powder diffraction (XRPD).

II. EXPERIMENTAL PROCEDURE

A. Sample preparation

A polycrystalline sample of perovskite with nominal composition $YAl_{0.25}Cr_{0.75}O_3$ was synthesized through a sol-gel combustion process. Details on the synthesis process are given in references [11, 12]. As reported in [12], the sample is monophasic with a refined chromium fraction of x_{Cr} = 0.73(1) apfu, meaning that the investigated sample has formula $YAl_{0.27}Cr_{0.73}O_3$.

B. Synchrotron X-ray powder diffraction

In situ high-pressure X-ray diffraction experiments were conducted at beamline ID27 at the European Synchrotron Radiation Facility. Hydrostatic pressure was generated up to 30.8 GPa on the sample using a diamond anvil cell (DAC) with diamond culet faces of 350 μm diameter. Powders were loaded into a preindented gasket hole (i.e., a rhenium foil of 50 μm thickness) with 150 μm diameter, and He as the pressure-transmitting medium [13]. A small single-crystalline ruby sphere was loaded into the cell in order to measure the pressure by means of the fluorescence method [14]. The wavelength of the monochromatic incident X-ray beam was λ = 0.3738 Å, which corresponds to the iodine K-edge. Debye-Sherrer rings were collected with a MAR 165circular CCD detector with an active imaging surface of 165 mm diameter and pixel size at CCD of 15 x 15 μm. The accessible angular range was within the limit imposed by the aperture of the diamond anvil cell (i.e., ca. 20° in 2θ).

Subsequently, the collected data were reduced and integrated radially over the full rings by the DIOPTAS program [15] using beam centre, detector tilt and sample to detector distance determined from a powder diffraction pattern of CeO_2 as standard, in order to obtain the conventional intensity vs. 2θ angle patterns. Furthermore, all the diffraction peaks of diamond and solid He (above 12 GPa) were masked. In order to check the goodness of the reduced data, a refinement of the unit-cell parameters was performed sequentially by SEQGSAS & SEQPLOT programs, within the EXPGUI-GSAS suite [16].

Rietveld refinements

The EXPGUI v.1251 interface [16] for the GSAS program [17] was used for Rietveld refinements. The structure refinement of the $YAl_{0.25}Cr_{0.75}O_3$ orthorhombic perovskite was carried out in the *Pnma* space group, starting from the structural model (i.e., cell parameters, fractional atomic coordinates and isotropic displacement parameters) of $YCrO_3$ [12]. The diffraction peak profile was modeled by a pseudo-Voigt function, which included Gaussian and Lorentzian broadening coefficients, plus an asymmetry contribution. Besides that, a shifted Chebyshev polynomial was employed to reproduce the background. The variation of the atomic coordinates with pressure have been refined up to 18.9 GPa, as difficulties in reliable extraction of the diffracted intensities was encountered for collected data at the highest pressures investigated. Furthermore, the above described synthesis procedure should guarantee a homogeneous distribution of Al and Cr ions within the *B* octahedral site. Albeit no indications of Al and Cr ordering at the *B* sites have been observed, the reported values for octahedral bond distances, bond angles, and volumes should be conservatively considered as an averaged value.

Unit-cell parameters (*a*, *b*, *c*, and *V*), atomic fractional coordinates (*x*, *y*, and *z*), and isotropic displacement parameters (U_{iso}) of $YAl_{0.25}Cr_{0.75}O_3$ up to 18.9 GPa are listed in Table 1, whereas a selection of interatomic bond lengths, bond angles, octahedral tilts, and polyhedral volumes are listed in Table 2. A set of representative Rietveld plots at various pressures are given in Figure 1.

Table 1. Unit-cell parameters (a, b, c, and V), atomic fractional coordinates (x, y, and z), and isotropic displacement parameters (U_{iso}) of $YAl_{0.25}Cr_{0.75}O_3$ perovskite up to 18.86 GPa. Fixed coordinated, A site: y = ¼; B site: $x = y = 0$, and z = ½; O1: y = ¼.

$YAl_{0.25}Cr_{0.75}O_3$ (space group *Pnma*; $Z = 4$)												
P (GPa)		0.05(5)	0.75(6)	1.44(9)	2.30(9)	3.32(9)	4.32(5)	4.93(7)	5.62(6)	6.36(8)	7.40(8)	8.48(9)
a (Å)		5.47679(69)	5.47191(32)	5.46479(33)	5.45783(32)	5.44998(33)	5.44187(31)	5.43623(31)	5.43117(32)	5.42591(33)	5.41793(33)	5.41023(36)
b (Å)		7.49161(91)	7.48471(42)	7.47589(43)	7.46592(42)	7.45545(43)	7.44438(41)	7.43732(41)	7.43027(42)	7.42302(43)	7.41211(43)	7.40192(47)
c (Å)		5.22700(65)	5.22191(30)	5.21544(31)	5.20844(30)	5.20079(31)	5.19302(29)	5.18801(29)	5.18287(30)	5.17757(31)	5.16974(31)	5.16223(33)
V (Å^3)		214.464(78)	213.867(36)	213.072(37)	212.232(36)	211.319(37)	210.376(34)	209.756(34)	209.155(35)	208.535(36)	207.608(36)	206.727(39)
A	x	0.06076(28)	0.06262(14)	0.06244(15)	0.06271(15)	0.06270(15)	0.06333(15)	0.06314(15)	0.06327(15)	0.06349(15)	0.06361(16)	0.06372(17)
	z	0.9826(5)	0.98675(33)	0.98616(33)	0.98643(34)	0.98642(35)	0.98658(35)	0.98656(34)	0.9871(4)	0.9868(4)	0.9872(4)	0.9868(4)
	U_{iso} (Å^3 × 100)	0.63(4)	0.56(2)	0.57(2)	0.56(2)	0.56(2)	0.53(2)	0.52(2)	0.53(2)	0.53(2)	0.53(2)	0.53(2)
B	U_{iso} (Å^3 × 100)	0.43(8)	0.34(5)	0.36(5)	0.36(5)	0.39(5)	0.42(5)	0.44(5)	0.42(5)	0.42(5)	0.41(5)	0.42(5)
O1	x	0.4640(5)	0.4622(8)	0.4633(8)	0.4633(9)	0.4627(9)	0.4618(9)	0.4634(9)	0.4633(9)	0.4625(9)	0.4628(9)	0.4622(10)
	z	0.0953(7)	0.0941(4)	0.0949(4)	0.0946(4)	0.0941(4)	0.0943(4)	0.0949(4)	0.0948(4)	0.0944(4)	0.0944(4)	0.0947(5)
	U_{iso} (Å^3 × 100)	2.04(30)	1.10(16)	1.10(16)	1.03(7)	1.14(17)	1.19(17)	0.95(17)	1.16(17)	1.28(18)	1.40(18)	1.47(19)
O2	x	0.3017(7)	0.2974(4)	0.2989(4)	0.2983(4)	0.2987(4)	0.2972(4)	0.2990(4)	0.2979(4)	0.2974(4)	0.2961(5)	0.2968(5)
	y	0.0521(8)	0.0563(4)	0.0551(4)	0.0555(4)	0.0551(4)	0.0563(4)	0.0553(4)	0.0562(4)	0.0567(4)	0.0578(4)	0.0570(4)
	z	0.6965(8)	0.7012(5)	0.6994(4)	0.7002(5)	0.6998(5)	0.7013(5)	0.6994(5)	0.7006(5)	0.7012(5)	0.7026(5)	0.7018(5)
	U_{iso} (Å^3 × 100)	2.49(28)	0.87(14)	1.05(14)	0.98(14)	1.27(15)	1.11(15)	1.16(15)	1.07(15)	1.00(15)	1.00(15)	1.05(16)

P (GPa)		9.61(9)	10.54(9)	11.63(6)	12.34(7)	13.31(8)	14.40(9)	15.38(9)	16.45(9)	17.65(9)	18.86(9)
a (Å)		5.40064(36)	5.39463(36)	5.38665(38)	5.38101(43)	5.37414(45)	5.36743(54)	5.36027(66)	5.35364(86)	5.34584(106)	5.33775(139)
b (Å)		7.38979(47)	7.38169(47)	7.37118(49)	7.36468(56)	7.35596(59)	7.34713(70)	7.33799(86)	7.32938(113)	7.32024(139)	7.30954(181)
c (Å)		5.15318(33)	5.14722(33)	5.13948(35)	5.13463(40)	5.12801(42)	5.12135(50)	5.11445(61)	5.10763(80)	5.10012(98)	5.09204(128)
V (Å^3)		205.661(39)	204.970(39)	204.068(41)	203.482(47)	202.720(49)	201.961(58)	201.170(70)	200.418(92)	199.582(113)	198.674(147)
A	x	0.06370(17)	0.06381(17)	0.06391(19)	0.06269(20)	0.06232(21)	0.06237(24)	0.06231(29)	0.0621(4)	0.0630(5)	0.0624(6)
	z	0.9869(4)	0.9868(4)	0.9866(4)	0.9873(5)	0.9862(5)	0.9865(6)	0.9863(7)	0.9879(9)	0.9883(11)	0.9906(17)
	U_{iso} (Å^3 × 100)	0.53(2)	0.53(2)	0.53(2)	0.57(3)	0.56(3)	0.56(3)	0.54(4)	0.52(5)	0.53(6)	0.51(7)
B	U_{iso} (Å^3 × 100)	0.42(5)	0.42(5)	0.41(6)	0.38(6)	0.40(7)	0.39(7)	0.45(9)	0.52(12)	0.51(14)	0.62(18)
O1	x	0.4613(10)	0.4610(10)	0.4601(11)	0.4633(12)	0.4647(13)	0.4625(14)	0.4630(17)	0.4589(22)	0.4558(25)	0.4558(32)
	z	0.0944(5)	0.0942(5)	0.0936(5)	0.0947(5)	0.0956(5)	0.0948(6)	0.0954(8)	0.0928(11)	0.0916(14)	0.0914(17)
	U_{iso} (Å^3 × 100)	1.49(19)	1.33(20)	1.50(21)	1.18(22)	1.06(23)	0.84(26)	0.87(32)	0.7(4)	1.2(5)	1.2(6)
O2	x	0.2967(5)	0.2971(5)	0.2971(5)	0.3004(5)	0.3012(6)	0.3010(6)	0.3012(8)	0.3018(10)	0.2991(13)	0.2996(16)
	y	0.0579(4)	0.0571(5)	0.0577(5)	0.0546(6)	0.0541(6)	0.0539(7)	0.0540(8)	0.0537(10)	0.0569(12)	0.0563(15)
	z	0.7019(5)	0.7015(6)	0.7015(6)	0.6979(6)	0.6970(6)	0.6972(7)	0.6970(8)	0.6964(11)	0.6993(14)	0.6987(18)
	U_{iso} (Å^3 × 100)	1.10(16)	1.15(17)	1.22(18)	1.49(20)	1.53(21)	1.42(24)	1.42(29)	1.4(4)	1.1(4)	1.0(6)

Table 2. Selection of polyhedral bond distances, i.e., Y□O and *B*□O in Å (where $B = Al_{0.25}Cr_{0.75}$), interoctahedral bond angles, i.e. *B*□O□*B* in °, □ and θ octahedral tilts in ° (where □ and θ represent rotations of octahedra about the pseudocubic $[001]_p$ and $[110]_p$ axes, respectively), and polyhedral volumes, i.e. $V(AO_{12})$ and $V(BO_6)$ in $Å^3$, from structural refinement of $YAl_{0.25}Cr_{0.75}O_3$ perovskite up to 18.9 GPa. Standard deviations are reported in parentheses.

$YAl_{0.25}Cr_{0.75}O_3$ (space group *Pnma*; *Z* = 4)										
P (GPa)	Y□O1	Y□O1	Y□O1	Y□O1	Y□O2 [x2]	Y□O2 [x2]	Y□O2 [x2]	Y□O2 [x2]	$^{XII}\langle Y□O\rangle$	$^{VIII}\langle Y□O\rangle$
0.05(5)	3.321(8)	2.286(9)	3.067(4)	2.269(6)	2.485(8)	2.634(8)	3.446(2)	2.256(2)	2.715(6)	2.413(7)
0.75(6)	3.333(4)	2.257(5)	3.083(2)	2.257(3)	2.445(4)	2.664(4)	3.434(1)	2.274(1)	2.714(3)	2.410(4)
1.44(9)	3.323(4)	2.263(5)	3.079(2)	2.251(3)	2.456(4)	2.648(4)	3.434(1)	2.266(1)	2.710(3)	2.407(4)
2.30(9)	3.319(4)	2.258(5)	3.075(2)	2.248(3)	2.446(4)	2.649(4)	3.427(1)	2.267(1)	2.706(3)	2.404(4)
3.32(9)	3.318(4)	2.251(5)	3.068(2)	2.249(4)	2.447(5)	2.641(4)	3.423(1)	2.263(1)	2.703(4)	2.400(4)
4.32(5)	3.321(4)	2.239(5)	3.067(2)	2.245(4)	2.428(4)	2.649(4)	3.417(1)	2.265(1)	2.699(3)	2.396(4)
4.93(7)	3.308(4)	2.247(5)	3.065(2)	2.238(4)	2.442(4)	2.633(4)	3.418(1)	2.256(1)	2.696(3)	2.393(4)
5.62(6)	3.306(4)	2.243(5)	3.064(2)	2.234(4)	2.430(4)	2.640(4)	3.413(1)	2.257(1)	2.694(3)	2.391(4)
6.36(8)	3.308(4)	2.236(5)	3.059(2)	2.236(4)	2.420(5)	2.643(4)	3.409(1)	2.257(1)	2.691(4)	2.389(4)
7.40(8)	3.302(4)	2.233(5)	3.056(3)	2.230(4)	2.405(5)	2.650(4)	3.402(2)	2.257(2)	2.687(4)	2.386(4)
8.48(9)	3.302(5)	2.226(5)	3.052(3)	2.229(4)	2.408(5)	2.639(5)	3.399(2)	2.253(2)	2.684(4)	2.382(4)
9.61(9)	3.300(5)	2.218(5)	3.046(3)	2.227(4)	2.399(5)	2.640(5)	3.397(2)	2.245(2)	2.679(4)	2.377(4)
10.54(9)	3.299(5)	2.213(6)	3.042(3)	2.227(4)	2.402(5)	2.631(5)	3.392(2)	2.244(2)	2.677(4)	2.374(4)
11.63(6)	3.299(5)	2.204(6)	3.034(3)	2.229(4)	2.394(5)	2.632(5)	3.390(2)	2.239(2)	2.673(4)	2.370(4)
12.34(7)	3.272(6)	2.225(7)	3.036(3)	2.212(5)	2.432(6)	2.597(6)	3.386(2)	2.229(2)	2.669(5)	2.369(5)
13.31(8)	3.260(6)	2.234(7)	3.029(3)	2.208(5)	2.434(6)	2.590(6)	3.385(2)	2.220(2)	2.666(5)	2.366(5)
14.40(9)	3.267(7)	2.218(8)	3.025(4)	2.210(6)	2.431(7)	2.586(7)	3.378(2)	2.220(2)	2.663(6)	2.363(6)
15.38(9)	3.261(8)	2.219(9)	3.023(4)	2.204(7)	2.428(8)	2.583(8)	3.376(2)	2.215(2)	2.659(6)	2.359(7)
16.45(9)	3.273(10)	2.191(12)	3.017(6)	2.211(9)	2.436(11)	2.573(10)	3.369(3)	2.213(3)	2.656(8)	2.356(9)
17.65(9)	3.288(12)	2.165(14)	3.012(7)	2.218(11)	2.401(13)	2.598(12)	3.366(4)	2.215(4)	2.654(10)	2.351(11)
18.86(9)	3.278(15)	2.162(18)	3.018(10)	2.203(15)	2.412(17)	2.584(16)	3.354(5)	2.214(5)	2.649(13)	2.348(15)

P (GPa)	*B*□O1	*B*□O2	*B*□O2	$\langle B□O\rangle$	*B*□O1□*B*	*B*□O2□*B*	$\langle B□O□B\rangle$	□	θ	$V(AO_{12})$	$V(BO_6)$
0.05(5)	1.948(3)	1.984(3)	1.962(3)	1.965(3)	148.09(24)	147.18(16)	147.64(20)	12.0(5)	16.6(5)	43.517(98)	10.099(20)
0.75(6)	1.946(2)	1.982(2)	1.960(2)	1.963(2)	148.19(24)	147.21(16)	147.70(20)	13.0(5)	16.5(5)	43.412(47)	10.055(11)
1.44(9)	1.944(2)	1.980(2)	1.958(2)	1.961(2)	148.11(24)	147.12(16)	147.62(20)	12.7(5)	16.6(5)	43.238(48)	10.030(11)
2.30(9)	1.941(2)	1.977(2)	1.955(2)	1.958(2)	148.18(24)	147.21(16)	147.70(20)	12.8(5)	16.5(5)	43.075(47)	9.983(11)
3.32(9)	1.938(2)	1.974(2)	1.952(2)	1.955(2)	148.26(24)	147.21(16)	147.74(20)	12.7(5)	16.5(5)	42.892(49)	9.937(12)
4.32(5)	1.936(2)	1.971(2)	1.949(2)	1.952(2)	148.08(24)	147.24(16)	147.66(20)	13.0(5)	16.6(5)	42.702(45)	9.892(11)
4.93(7)	1.934(2)	1.970(2)	1.948(2)	1.951(2)	148.12(24)	147.05(16)	147.59(20)	12.8(5)	16.6(5)	42.562(45)	9.877(11)
5.62(6)	1.932(2)	1.968(2)	1.946(2)	1.949(2)	148.14(24)	147.07(16)	147.61(20)	13.0(5)	16.6(5)	42.444(46)	9.845(11)
6.36(8)	1.930(2)	1.966(2)	1.944(2)	1.947(2)	148.15(24)	147.09(16)	147.62(20)	13.1(5)	16.5(5)	42.322(48)	9.812(12)
7.40(8)	1.927(2)	1.963(2)	1.941(2)	1.944(2)	148.18(28)	147.11(16)	147.65(23)	13.3(5)	16.5(5)	42.138(48)	9.764(12)
8.48(9)	1.925(2)	1.959(2)	1.938(2)	1.941(2)	148.05(28)	147.15(20)	147.60(24)	13.1(5)	16.6(5)	41.957(51)	9.725(12)
9.61(9)	1.922(2)	1.957(2)	1.935(2)	1.938(2)	148.01(28)	146.88(20)	147.45(24)	13.3(5)	16.6(5)	41.730(51)	9.686(12)
10.54(9)	1.920(2)	1.955(2)	1.933(2)	1.936(2)	148.02(28)	147.02(20)	147.52(24)	13.2(5)	16.6(5)	41.595(52)	9.647(13)
11.63(6)	1.917(2)	1.953(2)	1.931(2)	1.934(2)	148.09(32)	146.84(20)	147.47(27)	13.3(5)	16.6(5)	41.409(54)	9.609(13)
12.34(7)	1.915(3)	1.951(3)	1.929(3)	1.932(3)	148.19(28)	146.82(20)	147.51(24)	12.6(5)	16.5(5)	41.278(62)	9.593(15)
13.31(8)	1.913(3)	1.949(3)	1.927(3)	1.930(3)	148.10(28)	146.73(20)	147.42(24)	12.5(5)	16.6(5)	41.113(64)	9.567(15)
14.40(9)	1.911(3)	1.946(3)	1.924(3)	1.927(3)	148.05(32)	146.85(20)	147.45(27)	12.4(5)	16.6(5)	40.967(76)	9.523(18)
15.38(9)	1.909(4)	1.944(4)	1.921(4)	1.925(4)	147.95(36)	146.75(24)	147.35(31)	12.5(5)	16.6(5)	40.798(90)	9.495(20)
16.45(9)	1.905(5)	1.942(5)	1.919(5)	1.922(5)	148.16(44)	146.66(32)	147.41(38)	12.4(5)	16.5(5)	40.653(119)	9.451(27)
17.65(9)	1.903(6)	1.939(6)	1.917(6)	1.920(6)	148.08(52)	146.52(36)	147.30(45)	13.1(5)	16.5(5)	40.488(145)	9.407(32)
18.86(9)	1.900(7)	1.936(7)	1.914(7)	1.917(7)	148.12(64)	146.54(40)	147.33(53)	13.0(5)	16.5(5)	40.305(189)	9.364(42)

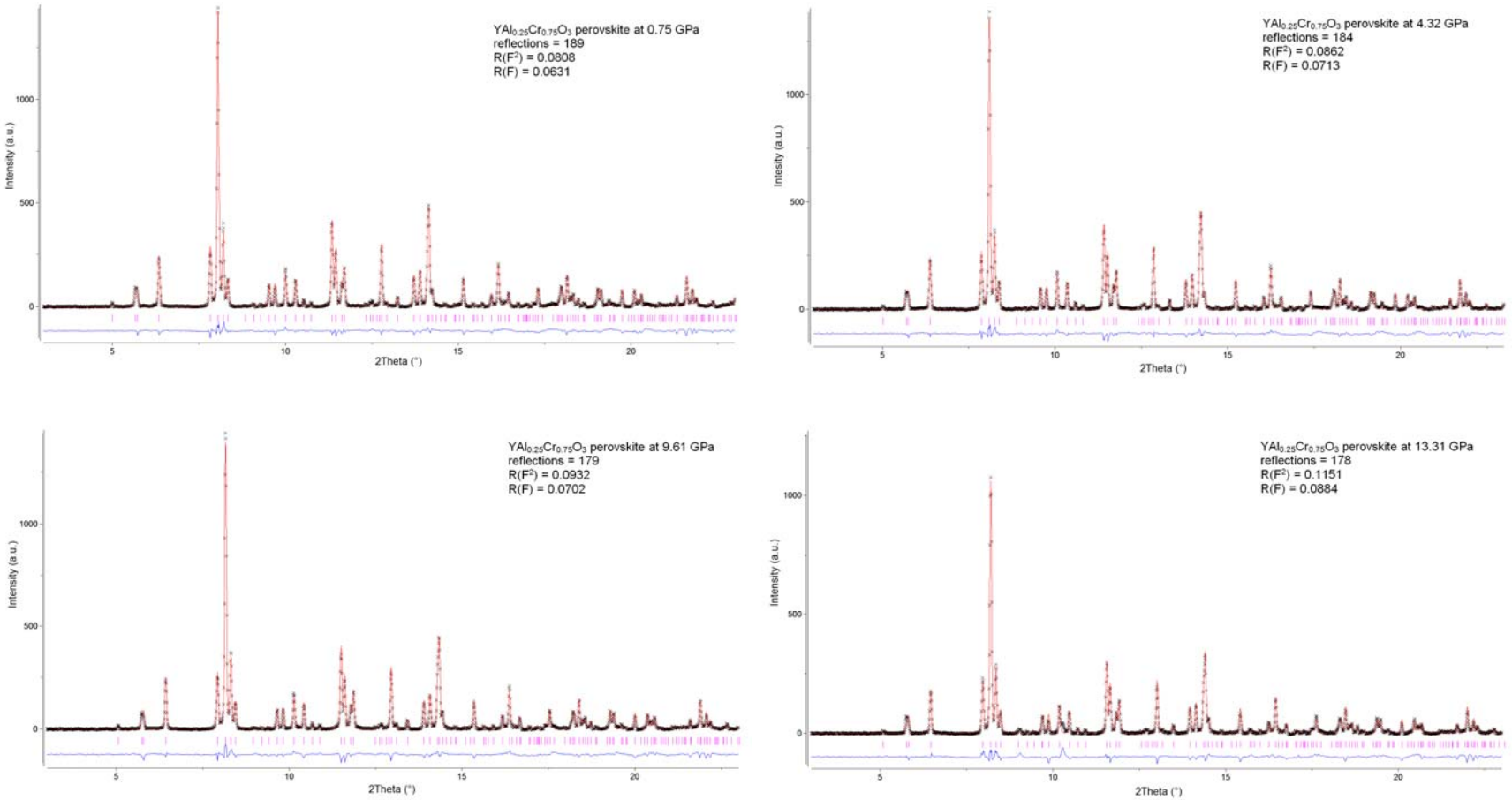

FIG. 1. Plot of the Rietveld refinements for $YAl_{0.25}Cr_{0.75}O_3$ perovskite at 0.75, 4.32, 9.61. and 13.31 GPa at room temperature ($\lambda = 0.3738$ Å). The experimental data are indicated by black crosses, the calculated pattern is the continuous red line, whereas the lower blue curve is the weighted difference between the observed and calculated patterns. Vertical ticks mark the position of reflections for perovskite in the *Pnma* space group.

III. RESULTS AND DISCUSSION

A. Elastic properties and EoS of $YAl_{0.25}Cr_{0.75}O_3$

Figure 2 shows the pressure dependence of both normalized unit-cell volume and axes. Data variation is continuous and smooth, and no evidence of phase transition is observed up to the maximum pressure investigated. The unit-cell axes define trends that are overlapped within the data uncertainties, meaning that $YAl_{0.25}Cr_{0.75}O_3$ compresses isotropically.

As a matter of fact, the fitting of the data to a Birch-Murnaghan third-order equation of state (BM3-EoS) by EosFit7-GUI [18] provides volumetric and axial moduli (the latter obtained by fitting the measured data with the same EoS to the cubes of each cell axes) almost identical. The volumetric bulk modulus (K_{T0}) and its pressure derivative (K'_0) are 212(1) GPa and 3.8(0.1), whereas the axial moduli (K_{d0}) and their pressure derivatives (K'_{d0}) are K_{a0} = 216(5) GPa, K_{b0} = 210(2) GPa and K_{c0} = 209(2) GPa, with K'_{a0} = 3.1(0.1), K'_{b0} = 5.0(0.1) and K'_{c0} = 3.5(0.1).

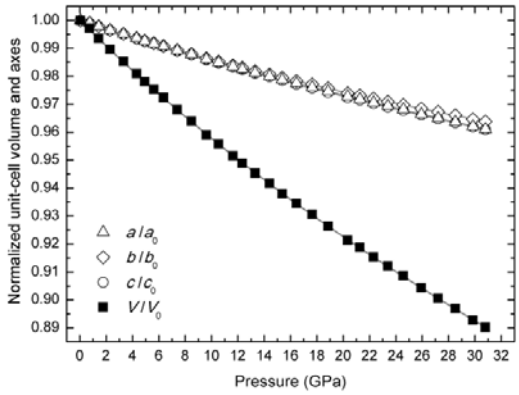

FIG. 2. Pressure dependence of both normalized unit-cell volume (filled squares) and unit-cell axes (open symbols) for $YAl_{0.25}Cr_{0.75}O_3$ perovskite oxide. Symbol sizes exceed the estimated uncertainties in measurements. Lines are the EoS fit to the data.

B. Normalized cell distortion factor with pressure of $YM^{3+}O_3$ compounds

The isotropic answer to the compressional regime for the perovskite $YAl_{0.25}Cr_{0.75}O_3$ is further highlighted in Figure 3, where the variation of the "*normalized cell distortion factor with pressure*" □ i.e., the rate of change with pressure of the cell distortion factor as defined by Sasaki et al. [19] normalized to the value calculated at ambient conditions (d_0), such as $d_{norm}(P) = 1/d_0 \cdot (\partial d/\partial P)_T$ [8, 20] □ is compared with that of $YM^{3+}O_3$ (M^{3+} = Ti, Cr, and Al) isotype compounds [7, 21], as well as with that of $GdFeO_3$ [22]. Here, all the possible lattice evolutions with pressure of orthorhombic perovskites (in which *A* and *B* cations have the same formal valence) are depicted. Specifically, for $YAlO_3$, $d_{norm}(P)$ decreases with increasing pressure, and thus, as indicated by first-principles calculations based on density functional theory [23], pressure leads this compound towards the cubic aristotype through a series of phase transitions. Conversely, the lattices of $YCrO_3$ and especially that of $YTiO_3$ become more distorted with increasing pressure (i.e. $d_{norm}(P)$ increases) suggesting a possible symmetry reduction at pressures higher than 60 and 30 GPa (i.e. above the maximum pressures investigated where symmetry changes were not detected [7, 24]). $YAl_{0.25}Cr_{0.75}O_3$ finds place at halfway; irrespective of the undergone compressional degree, this perovskite maintains its lattice distortion unchanged, equal to its initial value at ambient conditions.

Although subject to a modest decrease of the lattice distortion with increasing pressure, also the $GdFeO_3$ shows a lattice evolution comparable to that of $YAl_{0.25}Cr_{0.75}O_3$. Analysis of the unit cell parameter data shows that $GdFeO_3$ is slightly stiffer along [100], and thus that $GdFeO_3$ compresses almost isotropically [22].

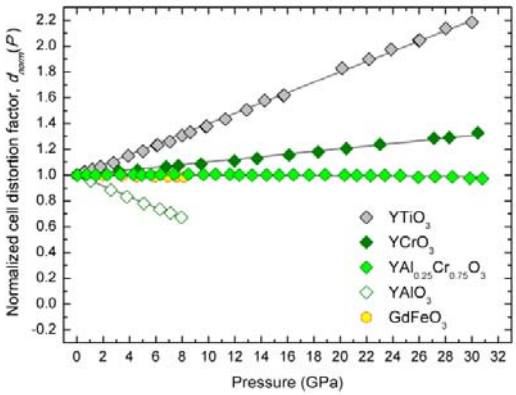

FIG. 3 (color online). Normalized cell distortion factor with pressure, $d_{norm}(P)$, as a function of pressure. Lines are linear fit to the data.

C. Structural evolution of $YAl_{0.25}Cr_{0.75}O_3$ perovskite at high pressure

Since the interplay between relative compressibility of the AO_{12} and BO_6 polyhedral sites and BO_6 octahedral tilting plays a key role in determining whether the perovskite structure becomes more distorted with increasing pressure, and it is fundamental in describing the thermodynamic processes associated with displacive phase transitions in perovskites, structural refinements under high pressure at room temperature were performed up to about 19 GPa.

Figure 4 illustrates the pressure dependence of polyhedral volumes V_A and V_B (A), of the two symmetry-independent B□O□B bond angles (B), and of the □ and θ octahedral tilts (C) for $YAl_{0.25}Cr_{0.75}O_3$.

Differently to what reported for any other orthorhombic perovskite (with no exception known), the polyhedral compressibility for both AO_{12} and BO_6 sites is exactly the same within the standard deviation. The parameters derived from P-V data by fitting a BM3-EoS, i.e. the polyhedral bulk modulus (K_{P0}) and its pressure derivative (K'_{P0}), are 210(13) GPa and 3.6(1.7) for the YO_{12} cubic sites and 202(14) GPa and 6.6(2.3) for the $(Al_{0.25}Cr_{0.75})O_6$ octahedra, respectively. This unusual and unique behavior can be readily explained by considering the absence of variation of B□O□B bond angles as well as the changeless degree of octahedral tilts with pressure (Figure 4B and 4C). As highlighted in the inset of Figure 4A, and reported in [22], the polyhedral compressibility of $GdFeO_3$ follows that of $YAl_{0.25}Cr_{0.75}O_3$, i.e. K_{A0} and K_{B0} are the same. At variance with $YAl_{0.25}Cr_{0.75}O_3$, $GdFeO_3$ tends to become less distorted with increasing pressure basically due to a little change in the Fe–O2–Fe angle with pressure but an increase of the Fe–O1–Fe tilting angle [22].

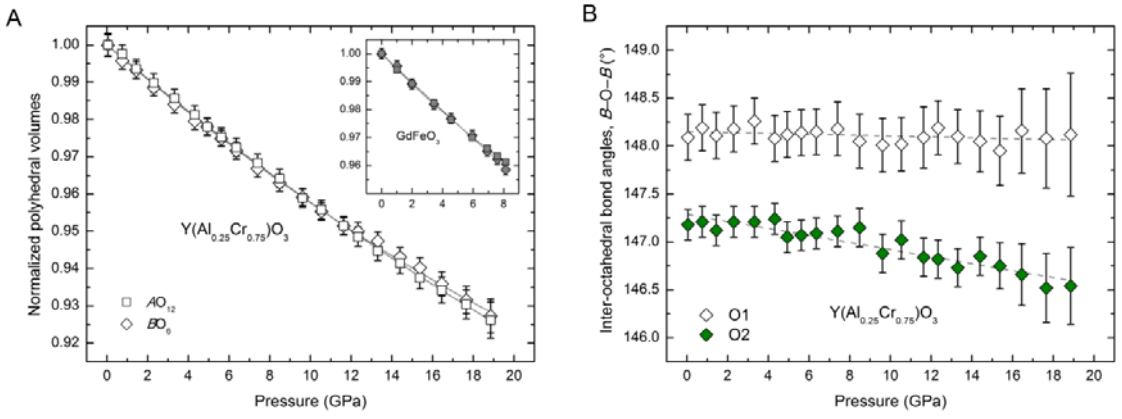

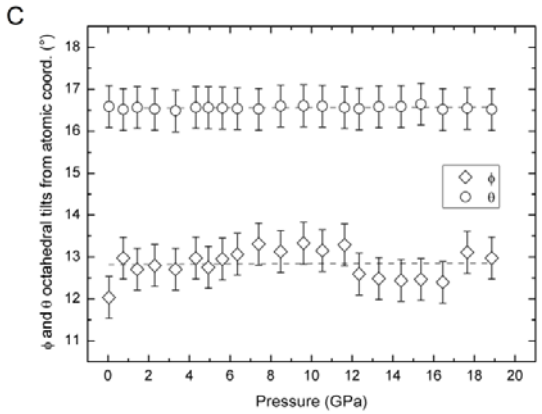

FIG. 4. Pressure dependence of the normalized polyhedral volumes (A), of the symmetry-independent *B*□O□*B* angles (B), and of □ and θ octahedral tilts achieved from atomic coordinates (C). Lines in A are the EoS fit to the data.

IV. CONCLUDING REMARKS

Overall picture – The $YM^{3+}O_3$ isotype series of orthorhombic perovskites offers a comprehensive overview of all the possible interactions between polyhedral compressibility and the variation of the octahedral tilting with pressure. Specifically, it follows that:

- As depicted in Figure 5A, $YAlO_3$ behaves as foreseen by the general rule as modified by Angel et al. [3], where the volume reduction due to a differential polyhedral compressibility, i.e. with the AO_{12} site stiffer than the BO_6 octahedron, is partially compensated by a decrease of the octahedral tilting [21]. The slope of the Clapeyron relation will be negative ($dT_c/dP = \Delta S/\Delta V < 0$).
- The absence of change in octahedral tilting sets $YAl_{0.25}Cr_{0.75}O_3$ at the boundary of the general rule [3] where the volume reduction with pressure is exclusively due to an isotropic polyhedral compression (Figure 5B). From a thermodynamic point of view, the latter situation can be seen as a possible asymptote at the Clapeyron relation for predicting the variation in transition temperatures of tilt transitions in perovskites. As a matter of fact, it implies a possible scenario where phase transitions could not take place. In order to clarify this engaging aspect, an X-ray diffraction study at high-temperature conditions has be planned to be performed on the $YAl_{0.25}Cr_{0.75}O_3$ perovskite compound.
- Antithetical to $YAlO_3$, $YCrO_3$ as well as $YTiO_3$ are characterized by a lattice distortion increase with pressure (Figure 3). This fact suggests that, for these compounds the volume reduction due to the compressibility of the polyhedral sites is not compensated by a decrease of the octahedral tilting (Figure 5C). Indeed, it is reported that the changes in the bond angles up to 16 GPa for $YTiO_3$ is of about 1° and that, the main octahedral bond angle is essentially pressure insensitive due to the opposite changes in the Ti–O1–Ti and Ti–O2–Ti bond angles [24]. Furthermore, albeit YO_{12} site is stiffer than TiO_6 octahedron when derived from a second-order BM-EoS fit to *P*-*V* data [20], when fitted by a BM3-EoS the situation is reversed and YO_{12} is more compressible than TiO_6, i.e. the polyhedral bulk moduli are 175(6) GPa and 199(11) GPa for the YO_{12} cubic sites and TiO_6 octahedra, respectively. Nevertheless, it should be pointed out that, at variance with Cr^{3+}, Ti^{3+} in $YTiO_3$ is a $3d^1$ system. The pressure dependence of orbital ordering physics has been shown to play an important role in $YTiO_3$ compound [24]. Anyway, $YCrO_3$ and $YTiO_3$ seem to violate the general rule as modified by Angel et al. [3], and follow the thermodynamic which identifies perovskites 2:4 ruled by a Clapeyron relation satisfied for $dT_c/dP = \Delta S/\Delta V > 0$.

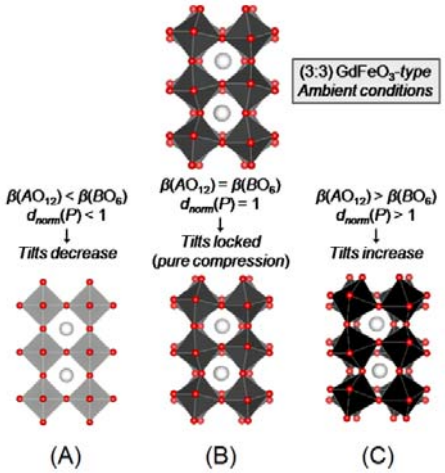

FIG. 5. Scheme of the possible polyhedral evolution of $GdFeO_3$type perovskites characterized by cations with the same formal charge at both cubic and octahedral site. The three possible pressure-dependence patterns are those followed by orthorhombic $YAlO_3$ (A), $YAl_{0.25}Cr_{0.75}O_3$ (B), and $YCrO_3$ (C).

Besides that, orthochromites are known for their ferroelectric features [25]. Although globally centrosymmetric (CS), at the short-range $YCrO_3$ is noncentrosymmetric (NCS) due to a Cr displacement of about 0.01 Å along the *c*-axis [26]. This local displacement bestows a polar state which is the origin of the $YCrO_3$ ferroelectricity. On the other hand, the ferroelectric features reported in orthorhombic YCrO3 are not fully understood [25].

In the last years, it is increasingly evident that a polar state and even ferroelectricity in CS perovskite structures derive from an octahedral tilting mismatch between blocks of layered perovskites or at the interface of perovskite oxides and superlattices grown as thin-films [2].

As reported by Benedek et al. [2], the strong coupling of oxygen rotations to the functional properties of a perovskite compound represents an opportunity to understand and create new functional materials that respond to an external perturbation in a useful way (e.g. multiferroics). Although theoretically this coupling can be managed with a high degree of accuracy, from an experimental point of view the mutual interaction between layers of octahedrally tilted perovskites subjected to an external perturbation can be easily tuned whether one of the layers is a "*locked-tilt perovskite*".

With reference to the specific case of $YCrO_3$, it can be speculated that its ferroelectric state could originate at the interface of two different octahedral tilting lattice domains. Whether this condition is maintained in $YAl_{0.25}Cr_{0.75}O_3$, the freezing of octahedral tilts can be extremely useful in the application and designing of new compounds where the structural features should not be subjected to the variation of external stresses.

Acknowledgements

The European Synchrotron Radiation Facility is acknowledged for provision of beamtime to proposal number CH-4541 at ID27 beamline. In particular, we are grateful to Dr. Volodymyr Svitlyk, beamline scientist during our experiment, for his suggestions and assistance in the experimental setting and procedure.

References

[1] T. S. Duffy, Nature **506**, 427 (2014).
[2] N. A. Benedek, A. T. Mulder, and C. J. Fennie, J. Solid State Chem. **195**, 11 (2012).
[3] R. J. Angel, J. Zhao, and N. L. Ross, Phys. Rev. Lett. **95**, 025503 (2005).

[4] T. Tohei, A. Kuwabara, T. Yamamoto, F. Oba, and I. Tanaka, Phys. Rev. Lett. **94**, 035502 (2005).
[5] G. A. Samara, T. Sakudo, and K. Yoshimitsu, Phys. Rev. Lett. **35**, 1767 (1975).
[6] M. Guennou, P. Bouvier, B. Krikler, J. Kreisel, R. Haumont, and G. Garbarino, Phys. Rev. B **82**, 134101 (2010).
[7] M. Ardit, G. Cruciani, M. Dondi, M. Merlini, and P. Bouvier, Phys. Rev. B **82**, 064109 (2010).
[8] M. Ardit, M. Dondi, and G. Cruciani, in *Lattice Distortion Upon Compression in Orthorhombic Perovskite: Review and Development of a Predictive Tool*, edited by S. V. Krivovichev, Minerals as Advanced Materials II (Springer, Berlin, 2011).
[9] N. A. Benedek and C. J. Fennie, Phys. Rev. Lett. **106**, 107204 (2011).
[10] P. V. Balachandran, D. Puggioni, and J. M. Rondinelli, Inorg. Chem. **53**, 336 (2014).
[11] M. Blosi, S. Albonetti, M. Dondi, A. L. Costa, M. Ardit, and G. Cruciani, J. Sol-Gel Sci. Technol. **50**, 449 (2009).
[12] G. Cruciani, M. Ardit, M. Dondi, F. Matteucci, M. Blosi, M. C. Dalconi, and S. Albonetti, J. Phys. Chem. A **113**, 13772 (2009).
[13] M. Mezouar, W. A. Crichton, SBauchau, F. Thurel, H. Witsch, F. Torrecillas, G.Blattmann, P. Marion, Y. Dabin, J. Chavanne, O. Hignette, C. Morawe, and C. Borel, (2005) J. Synchrotron Rad. **12**, 659 (2005).
[14] H. K. Mao, J. Xu, and P.M. Bell, J. Geophys. Res. Solid Earth **91**, 4673 (1986).
[15] C. Prescher and V. B. Prakapenka, High Pressure Res. **35**, 223 (2015).
[16] H. Toby, J. Appl. Cryst. **34**, 210 (2001).
[17] A. C. Larson and R. B.Von Dreele, *General Structure Analysis System* (GSAS). Los Alamos National Laboratory Report No. LAUR 86 748. Los Alamos National Laboratory, New Mexico, USA,1988.
[18] J. Gonzales-Platas, M. Alvaro, F. Nestola, and R. J. Angel, J. Appl. Cryst. **49**, 1377 (2016).
[19] S. Sasaki, C. Prewitt, and R. Liebermann, Am. Mineral. **68**, 1189 (1983).
[20] M. Ardit, J. Phys. Chem. Solids **87**, 203 (2015).
[21] N. L. Ross, J. Zhao, and R. J. Angel, J. Solid State Chem. **177**, 1276 (2004).
[22] N. L. Ross, J. Zhao, and R. J. Angel, J. Solid State Chem. **177**, 3768 (2004).
[23] X. Wu, S. Qin, and Z. Wu, J. Phys.: Condens. Matter **18**, 3907 (2006).
[24] I. Loa, X. Wang, K. Syassen, H. Roth, T. Lorenz, M. Hanfland, and Y.-L. Mathis, J. Phys.: Condens. Matter **19**, 406223 (2007).
[25] R.Saha, A. Sundaresan, and C. N. R. Rao, Mater. Horiz. **1**, 20 (2013).
[26] K. Ramesha, A. Llobet, Th. Proffen, C. R. Serrao, and C. N. R. Rao, J. Phys.: Condens. Matter **19**, 102202 (2007).